Peer-Reviewed Technical Communication

Measurement of Sound Speed in Fine-Grained Sediments During the Seabed Characterization Experiment

Jie Yang and Darrell R. Jackson

***Abstract*—The Seabed Characterization Experiment was carried out from March 5 to April 10, 2017 (SBCEX17) on the New England Mud Patch, approximately 90 km south of Martha's Vineyard. The SBCEX17 experimental site covers an area of 11 km × 30 km with water depth in the range of 75–80 m. The Sediment Acoustic-speed Measurement System (SAMS) is designed to measure sediment sound speed and attenuation simultaneously over the surficial 3 m of sediments. During SBCEX17, SAMS was successfully deployed at 18 sites, which were chosen to coincide with coring locations, with the goal of developing a geoacoustic model for the study area. In this article, a summary of SAMS operation during SBCEX17 is presented, as well as preliminary results for sediment sound speed and its spatial variation in the frequency band of 2–10 kHz. It is found that in mud, the sound-speed ratio is in the range of 0.98–1. Little dispersion was observed in this frequency band. Using the preliminary SAMS sound-speed results measured at different depths, the sound-speed gradient in mud within the surficial 3 m favors an exponential rather than a linear dependence at SBCEX17 site. Large gradients are observed for depth shallower than 1.5 m. For the sandy basement beneath the mud layer, the sound-speed ratio is as high as 1.105.**

***Index Terms*—Geoacoustic modeling, mid-frequency, mud, SBCEX17, sediment sound speed, sound speed gradient.**

I. Introduction

SEDIMENT geoacoustic properties, which are the most important parameters for predicting sound propagation and reverberation in many cases, are difficult to acquire directly, especially in the low- to midfrequency band. *In situ* measurements of sediment properties were first made in the 1950s [1]–[8] for water depths ranging from tens of meters to a maximum of 1235 m [2]. Penetrating probes were pioneered with the goal of building a geoacoustic model for the seafloor [9]. In these early measurements, sediment properties were obtained at penetration depths of tens of centimeters in the frequency range of several kilohertz to 100 kHz. A wide range of sediment types were sampled from clayey silt to sand.

Recently, extensive *in situ* measurements of sediment properties have been conducted for the ocean acoustics community in sandy sediments and the majority are closely related to major sediment acoustics field experiments sponsored by the U.S. Office of Naval Research, Arlington, VA, USA. The *in situ* measurement results were summarized in [10]–[18] for the Sediment Acoustic Experiment in 1999 and 2004 (SAX99/04), [19]–[20] for the Shallow Water 2006 (SW06), and the Target and Reverberation Experiment in 2013 (TREX13) [21]–[22]. In addition to work related to major field trials, descriptions of *in situ* measurement efforts can also be found in [23]–[25]. These measurements were conducted from a few hundred hertz to a few hundred kilohertz to study the frequency dependencies of sediment sound speed and attenuation. Sediment acoustic models have been proposed for such frequency dependencies and representative efforts can be found in [26]–[30].

In contrast, mud properties, including subbottom layering, sound-speed gradients due to compaction, and gas content, are of great interest and importance to sound propagation and reverberation and as yet not well understood. Historical *in situ* data and investigations on mud or fine-grained sediment properties include work from [1]–[8], [31], and [32]. Sediment sound-speed ratio in mud was often found to be less than unity [1]–[4], [31], [32], and sound-speed gradients were often observed [5]–[8], [31]. Attenuation measurements were reported in [1], [3], [4], and [31]. It has been shown that reliable attenuation records are challenging to obtain in mud due to primitive techniques and complication from ambient noise [33]. With limited understanding and measurement of the geoacoustic properties in mud, sediment acoustic modeling is currently an ongoing research topic [34].

The Seabed Characterization Experiment was carried out from March 5 to April 10, 2017 (SBCEX17) on the New England Mud Patch, about 90 km due south of Martha's Vineyard. The main scientific goals of SBCEX17 are to discover the physical mechanisms that control sound propagation in fine-grained sediments and assess inversion and statistical inference techniques and their uncertainties in such sediments. Fig. 1 shows the experimental site, highlighted with a green box with bathymetric contours in the background. The main experimental area is 11 km × 30 km in size with water depth ranging from 75 to 80 m.

Two survey cruises were conducted in 2015 and 2016 aimed at providing an overview of the environment at the experimental site. During the 2015 cruise, a chirp sonar survey was conducted to give a three-dimensional map of the bottom structure in the form of two-way travel time (TWTT) [35] (see Fig. 2, bottom panel). In addition, during the two survey cruises, piston, vibracores, and acoustic cores were obtained and their locations were labeled on the TWTT map as well [36]–[38].

During SBCEX17, *in situ* measurements of sediment sound speed and attenuation in the experimental area were carried out in the frequency band of 600 Hz–10 kHz, using the Sediment Acoustic-speed Measurement System (SAMS). SAMS was successfully deployed at a total of 18 sites, which were chosen to coincide with the coring locations. A combination of direct measurements, such as cores and SAMS, as well as chirp sonar data can be used to build a geoacoustic model at the study site to facilitate the development of physics-based sediment acoustic models.

Manuscript received December 20, 2018; revised June 29, 2019, August 3, 2019, and August 16, 2019; accepted October 2, 2018. Date of publication November 7, 2019; date of current version January 13, 2020. This work was supported by the Ocean Acoustics, Office of Naval Research under Grant N00014-16-1-2782. *(Corresponding author: Jie Yang.)*

Guest Editor: P. Wilson.

The authors are with the Applied Physics Laboratory, University of Washington, Seattle, WA 98105 USA (e-mail: jieyang@apl.washington.edu; drj12@uw.edu).

Digital Object Identifier 10.1109/JOE.2019.2946004

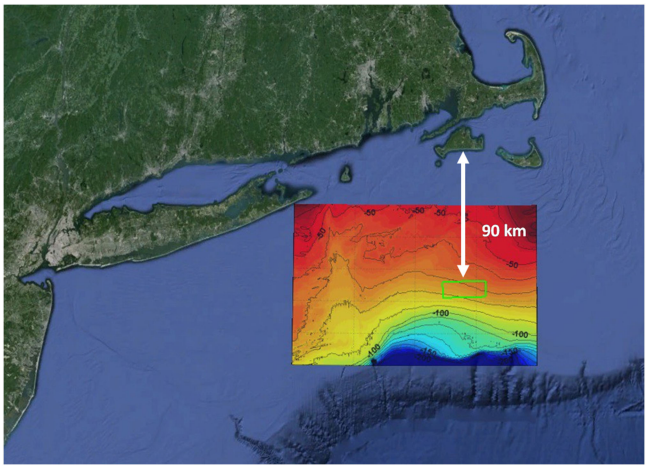

Fig. 1. SBCEX17 experimental site on the Mud Patch of New England. The study site, highlighted with the green box, is about 90 km south of Martha's Vineyard. The background color represents bathymetric contours using data from the National Oceanic and Atmospheric Administration bathymetry database.

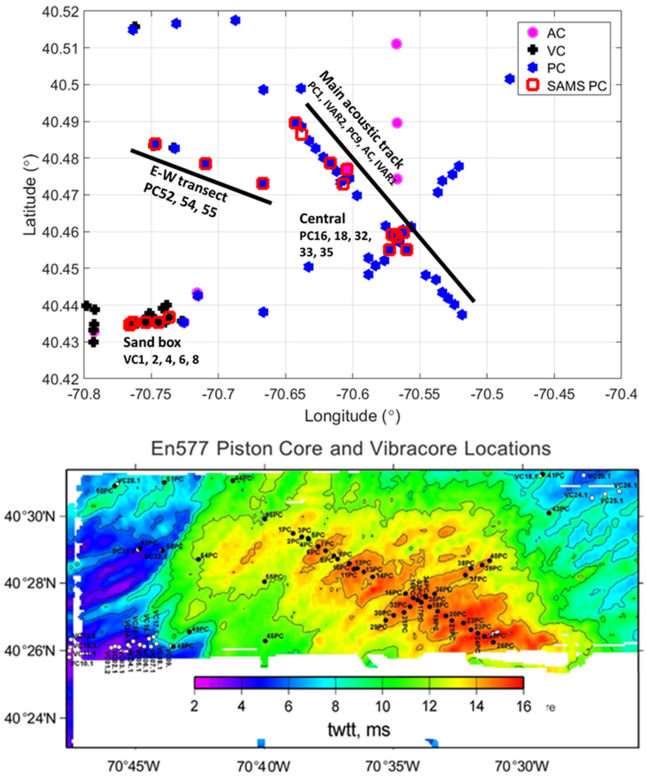

Fig. 2. Top panel: SBCEX17 experimental site with four types of direct measurement locations overlaid, including acoustic (magenta), piston (blue), vibracores (black), and Sediment acoustic-speed measurement system (SAMS) (red). The four priority areas and site names where SAMS data were taken are shown. Bottom panel: TWTT map of surficial mud layer with piston and vibracore locations. (Bottom panel picture courtesy of John Goff.)

This article is organized as follows. In Section II, system description and deployment information, as well as acoustic data, are presented. In this article, a time-of-flight method is adopted to obtain sound speeds and, therefore, all sound-speed results presented here are path-averaged sound speeds. The technique to obtain path-averaged sediment sound speed is shown in Section III. In this article, sediment sound-speed results in the frequency band of 2–10 kHz are presented. A full report of sediment sound speed and attenuation in the frequency band of 600 Hz–10 kHz will be the subject of a follow-on effort. Using SAMS results taken at different penetration depths in mud, a preliminary model for sediment sound speed versus depth is presented in Section IV, followed by the summary in Section V. A transducer model is presented in Appendix for source and receiver responses when immersed in different media, i.e., water versus mud, to help understand the acoustic data taken during SBCEX17.

II. Sediment Acoustic Data

During SBCEX17, SAMS was successfully deployed at 18 sites. Sediment sound speed was measured for the surficial 3 m at sites with varying mud layer thickness, as well as at sites that included penetration into the sandy basement [35]. These sites were chosen to coincide with acoustic, piston, and vibracore locations [36]–[38] (see Fig. 2), with the goal of developing a geoacoustic model for the study site.

A. System Description

SAMS, shown in Fig. 3, is designed to simultaneously measure sediment sound speed and attenuation over the upper 3 m of sediments. The system is about 4.8 m tall and 5 m wide between the end points of the triangular base and the extension arm [21]. SAMS has two independent and interchangeable drill systems: one employs a suction mechanism and the other a water jet. The suction system gives minimal disturbance to the medium around the penetrating probe, whereas the water jet system can help penetrate consolidated shell/sand layers. During SBCEX17, both systems were used: the suction system was used for the majority of the sites with thick mud layers, whereas the water jet system was used to penetrate the sandy basement. Typically, it took about 20 min for SAMS to be lowered to the seafloor, about 80 m below *R/V Sharp*, while it was in dynamic positioning mode. The center probe was then drilled into the sediment through motor control. Once at a desired depth, the data taking usually takes 40 min, and upon completion, data are transferred to the surface for analysis.

There are ten sources and one receiver on the SAMS tower. The ten sources include eight ITC1032s, one ITC1007, and one low-frequency source PS800. ITC1032 and ITC1007 cover a frequency band of 2–10 kHz, and data from these two sources will be the focus of this article. The acoustic receiver is a ring transducer at the tip of the center probe. The inset on the top right corner of Fig. 3 depicts the deployment conditions during SBCEX17, with all sources and receiver buried in mud.

The receiver penetration depth was recorded through an encoder, which measures depth by counting turns as the center shaft rotates to go down with submillimeter resolution. The penetration depth ranges from 0 m to maximum extension of 3 m, referenced to the SAMS frame. As mentioned earlier, SAMS sank into the soft sediments by 30–50 cm for all deployments and, therefore, all measurements were carried out within the 0.4–3.4-m depth range in sediments, relative to the water–sediment interface (see Table I; nominal 0.4-m sinking depth was used). When the probe is at penetration depths of 1.5 and 3 m, the grazing angle ranges for the ten source–receiver pairs are 27°–45° and 45°–68°, respectively, with sources ranging 1.2–3 m horizontally from the receiver probe.

A camera was installed on the triangular base of the tower and the footage was viewed in real time on board the ship. The real-time camera feed helps ensure safety during deployment and recovery and provides a qualitative view of surficial sediments and biological activity. In

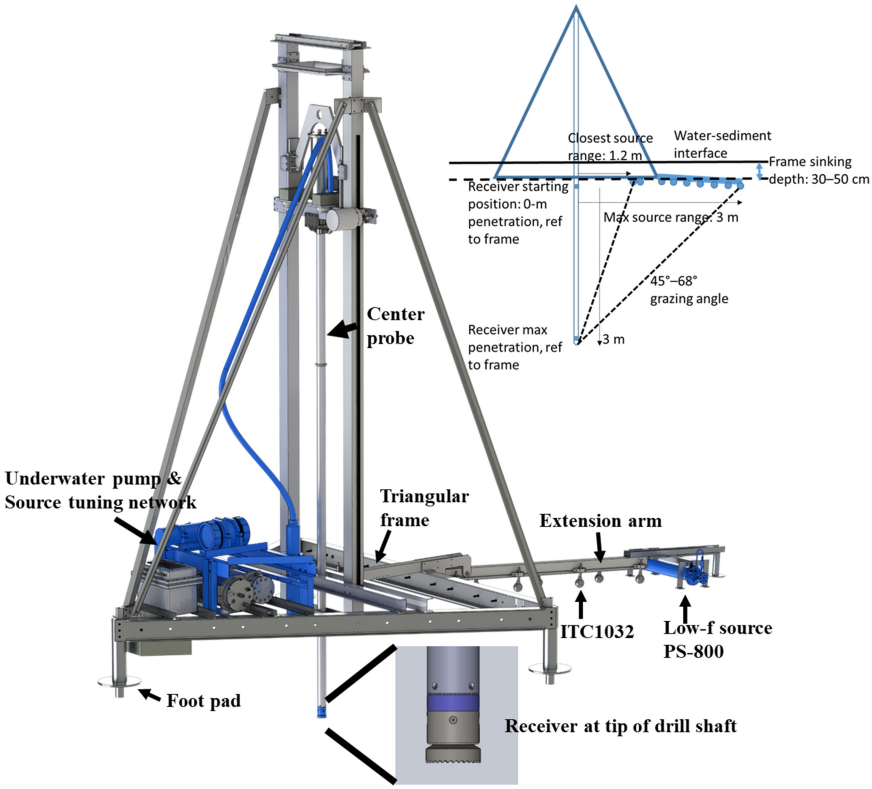

Fig. 3. SAMS: There are six ITC1032 and one ITC1007 sources on the extension arm and two ITC1032 sources under the triangular frame. A low frequency source PS800 is at the end of the extension arm. A ring transducer (receiver) is at the tip of the center probe that is drilled into the sediment under motor control. The inset shows the system geometry and grazing angle range when the probe is at its maximum penetration depth of 3 m. Receiver penetration depth is referenced to the frame, in the range of 0–3 m. Since SAMS sank into the soft sediment for all deployments, the source/receiver depths relative to the water–sediment interface shown in Table I have a nominal sinking depth of 40 cm taken into account.

addition, based on the camera footage, SAMS was observed to sink 30–50 cm into the mud for all deployments.

A conductivity-temperature-density (CTD) unit was fastened onto the SAMS frame throughout the experiment. The CTD unit was about 1 m above the water–sediment interface, with the frame sinking depth taken into account. From March 23 to April 6, the water sound speed near the seabed varied from 1470 to 1473 m/s (see Table I).

B. SAMS Deployments During SBCEX17

During SBCEX17, four priority areas were chosen and they are the following:

1) the central area;
2) the northwest (NW) section of the main acoustic track;
3) east–west (E-W) transect with transition into shallow mud layer to the west;
4) the "sand box" area with sandy intrusion as close to 1.5 m below the water–sediment interface (see Fig. 2; top panel).

These sites were chosen to study the spatial variation of sediment sound speed in both range and depth and, specifically, its relation with the following:

1) mud layer thickness;
2) sound-speed depth structure or its gradient in mud;
3) transition from mud into sandy basement.

Details of all deployments are listed in Table I, including the closest core location, SAMS GPS coordinate, penetration depth, source/receiver depths, and water sound speed about 1 m above the seafloor. At some of the sites, acoustic data were taken at two penetration depths, usually one near 1.5 m and the other at maximum penetration of 3 m. Note that the penetration depth is the relative depth between receiver and fixed source plane, whereas the source/receiver depths are referenced to the water–sediment interface and have the 30–50-cm system sinking depth taken into account.

C. Acoustic Data Obtained Using ITC1007 and ITC1032

As mentioned earlier, for all deployments at SBCEX17, SAMS sank about 30–50 cm into the soft surficial sediment. The fact that all sources and the receiver were buried in mud contributed collectively to the high quality of the acoustic data. In such cases, sound does not have to couple through the water–sediment interface as it does when the frame sits on the ocean bottom (with sources above water–sediment interface). In addition, the relatively homogeneous soft sediment enhances the strength and quality of the signal as will be seen.

During the experiment, Gaussian pulses with 1-kHz bandwidth were used with center frequencies in the range of 2–10 kHz in 500-Hz increments. During the experiment, every transmitted signal was repeated three times. The three received signals were observed to be almost identical and, therefore, only the mean signals are shown here. An example is shown in Fig. 4, using the 2–3-kHz Gaussian pulse. To reduce edge effects, the Gaussian envelope is allowed a 2-ms time window, with the Gaussian signal peak lined up at the 1-ms center. In Fig. 4, the acoustic signals are Gaussian filtered and the filter has a full 3-dB bandwidth of 1 kHz. Filtered data are shown in blue, whereas their envelopes are shown in red. Sources 1–8 are ITC1032s, whereas source 9 is an ITC1007. The horizontal distances between sources 1–9 and the

TABLE I
SAMS DEPLOYMENT INFORMATION DURING SBCEX17

SAMS site number	Core number	Date	Latitude (°)	Longitude (°)	Penetration depth (m)*	Source/receiver depths (m)** S – R	Water sound speed at bottom (m/s)
1	PC 33	3/24	40.4585	70.5678	1.500 2.383	0.4 – 1.900 0.4 – 2.783	1470.6
		3/24	0.4586	70.5676	3.019	0.4 – 3.419	1470.5
2	PC 16	3/27	40.4592	70.5708	2.726	0.4 – 3.126	1471.2
3	PC 18	3/27	40.4550	70.5600	2.432	0.4 – 2.832	1471.9
4	PC 32	3/28	40.4550	70.5727	2.570	0.4 – 2.970	1472.6
5	PC 35	3/28	40.4598	70.5604	1.500	0.4 – 1.900	1472.6
6	IVAR#2	3/28	40.4865	70.6383	1.500 2.570	0.4 – 1.900 0.4 – 2.970	1471.8
7	AC	3/28	40.4774	70.6035	2.258	0.4 – 2.658	1472.3
8	IVAR#1	3/30	40.4730	70.6075	2.420	0.4 – 2.820	1473.2
9	PC 1	3/30	40.4944	70.6527	2.405	0.4 – 2.805	1473.2
10	PC 9	3/30	40.4786	70.6170	2.382	0.4 – 2.782	1473.3
11	PC 55	3/30	40.4732	70.6668	2.276	0.4 – 2.676	1473.3
12	PC 54	3/31	40.4785	70.7097	1.215 3.034	0.4 – 1.615 0.4 – 3.434	1473.3
13	VC 1	4/3	40.4347	70.7661	1.522 2.897	0.4 – 1.922 0.4 – 3.297	1473.1
14	VC 4	4/3	40.4353	70.7541	1.531 3.030	0.4 – 1.931 0.4 – 3.430	1473.0
15	VC 2	4/3	40.4353	70.7636	1.506 2.882	0.4 – 1.906 0.4 – 3.282	1473.0
16	VC 6	4/3	40.4354	70.7446	1.552 3.030	0.4 – 1.952 0.4 – 3.430	1473.0
17	VC 8	4/4	40.4367	70.7368	1.500 3.035	0.4 – 1.900 0.4 –3.435	1473.0
18	PC 52	4/5	40.4838	70.7472	1.496 3.034	0.4 – 1.896 0.4 – 3.434	1473.5

PC: piston core, VC: vibracore, AC: acoustic core, and IVAR: intensity vector autonomous recorder.
*Penetration depth: receiver depth relative to SAMS frame.
**Source/receiver depths: depths relative to the water–sediment interface (with nominal 0.4-m sinking depth added, see Fig. 3 inset).

receiver range from 1.23 to 2.96 m. Signal amplitudes in Fig. 4 are normalized with reference to that of source 1, the closest ITC1032. Source 9, ITC1007, has a higher source level than those of ITC1032s, resulting in a higher signal amplitude. For sources that are directly under or close to the frame (sources 1–3), trailing arrivals scattered

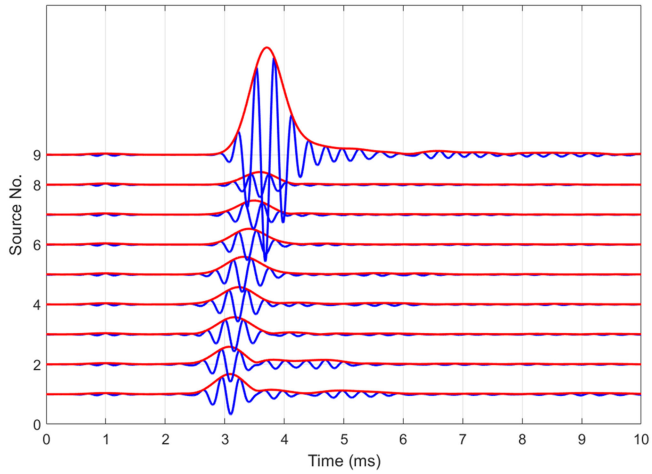

Fig. 4. Data taken during SBCEX17, with sources 1–8 ITC1032s and source 9 an ITC1007. Waveform used: 2–3-kHz Gaussian pulse. Signal amplitudes are normalized with reference to source 1.

from the frame can be observed, whereas sources further away are much less affected.

Interestingly, when comparing signal amplitudes between in-water and in-sediment data, it was found without exception that the signal amplitude with sources and receiver in sediment is higher than that when both are in water, given the same geometry. Fig. 5 shows the comparison between the in-water and in-sediment data for both ITC1032 (left) and ITC1007 (right) at a deep mud site, PC9. The in-water (blue) and in-sediment (red) data were taken at penetration depths of 2.384 and 2.382 m, respectively. For PC9, the in-sediment data slightly lag behind the in-water data, indicating a lower sound speed. Moreover, both panels show that the in-sediment data have higher amplitudes than their in-water counterparts. The minute difference in receiver depth (0.2 cm) cannot account for the 23% amplitude increase for the in-sediment data.

To understand the source performance when buried, a transducer model was developed for sources immersed in water or in mud, referred to as before and after burial cases in later text. Similar analysis was carried out for the acoustic receiver. Details of the transducer model and modeling results are given in the Appendix. The modeling of source performance is essential to understand both amplitude and phase changes for sources immersed in different media, which will impact both sound speed and attenuation analyses.

The results presented in this article are limited to the sediment sound-speed results for ITC1032 and ITC1007 since the parameters needed for the transducer model are only available for these two sources. Preliminary transducer modeling results show negligible phase change for ITC1032, ITC1007, and the receivers before and after burial in the frequency band of 2–10 kHz. As demonstrated in the Appendix, for typical SAMS propagation path lengths in the range of 2–4.3 m, this phase change would result in a maximum of 0.3% sound-speed correction. Though small, this slight phase change was included in all sound-speed calculations presented in this article.

III. SOUND-SPEED RESULTS IN FINE-GRAINED SEDIMENTS

Path-averaged sediment sound-speed results are presented for the four priority areas described in Section II. A time-of-flight method is adopted to obtain the path-averaged sound speeds over relevant propagation paths. Results show small variation for sound speeds in mud. For sites with data taken at two or more penetration depths, a simple two-layer model was built to investigate the averaged sound

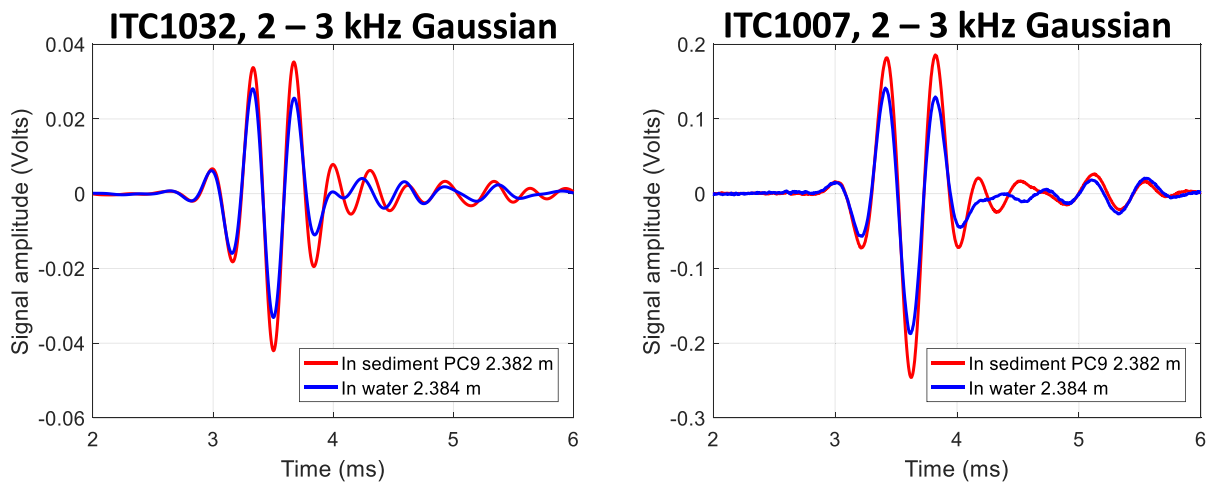

Fig. 5. Comparison between in-water and in-sediment data from ITC1032 (left) and ITC1007 (right) using the 2–3 kHz Gaussian signal at a deep mud site, PC9. The in-water and in-sediment data were taken at penetration depths of 2.384 and 2.382 m, respectively, with receiver depth differing by 0.2 cm.

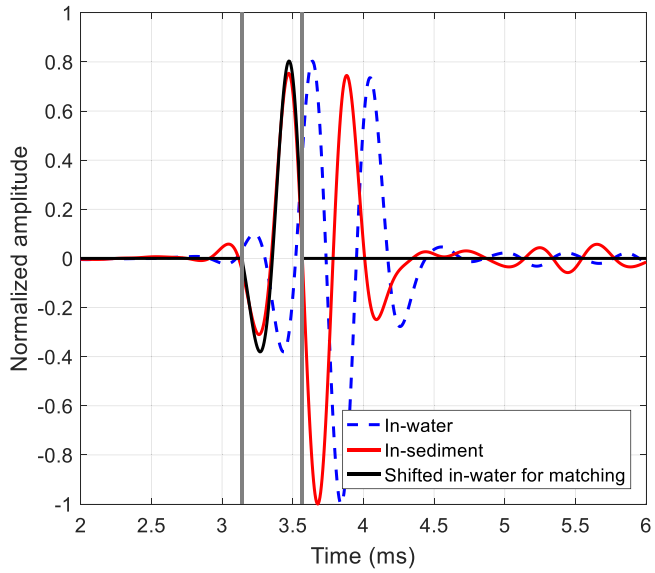

Fig. 6. Example of best matching both phase and amplitude between in-water and in-sediment data using ITC1007. Waveform: 2–3-kHz Gaussian pulse. Blue: in-water data at a receiver depth of 2.886 m. Red: in-sediment data at a receiver depth of 2.897 m at VC1 location. Black: shifted early part of in-water data to match the in-sediment within the matching time window marked by the gray lines. VC1: site with sandy intrusion.

speeds in both layers as a crude estimate of sound-speed gradient within the surficial 3 m.

A. Method to Obtain Sound Speed

To obtain signal arrival time, both phase and amplitude information of the early part of the signal were used, when there should be little contamination by unwanted arrivals. This was carried out by best matching both phase and amplitude of the early part of the signal between in-water and in-sediment data that were taken with close-to-the-same geometries.

The process of phase and amplitude matching between in-water and in-sediment signals is demonstrated in Fig. 6 using data from ITC1007. The in-water data were taken at the penetration depth of 2.886 m (see Fig. 3 inset for system geometry), whereas the in-sediment data were taken at 2.897 m (VC1 location). The blue and red curves represent in-water and in-sediment data; the black curve is the best match between the two for the part of the signal bounded by the two gray lines. Through best matching, the time difference between the two signals can be obtained. Since the geometry of the system is known, the time difference corresponds to the sound-speed difference between the two media. In addition, a slight correction is made to account for the delay of the transmitted signal due to immersion in the sediment (see the Appendix). With the sound speed in water measured using an on-frame CTD, the path-averaged sediment sound speed can be obtained.

B. Path-Averaged sound-Speed Results at the Four Priority Areas

The path-averaged sediment sound-speed results are presented as sound-speed ratios, i.e., the ratio between sound speed in sediment and in water. The in-water sound speed was measured using the on-frame CTD, as shown in Table I, for each site. The sound-speed ratios and their uncertainties for the four priority areas are presented here, starting from the central area. Note, results in Fig. 7 and later in Fig. 8 are mostly in the penetration depth range of 2–3 m (see Table I for penetration depths). For sites that have multiple penetration depths, the results represent mean sound-speed ratio averaged over all penetration depths, if not stated otherwise. They are used here to first study the general sound-speed variation among the four priority areas. The depth dependence of sound speed in mud is presented later in this section.

Measurements at the five sites in the central area yield similar sound-speed ratios [see Fig. 7(a)] with the mean sound-speed ratio in the range of 0.99–1. Little dispersion is observed in the frequency band of 2–10 kHz. The uncertainty bars represent one standard deviation of sound-speed results obtained using the nine source–receiver pairs. It is interesting that the other five sites, along the NW part of the main acoustic track, show similar variation among sites, but the overall sound-speed ratio is less than that in the central area by 0.5% or 7.4 m/s [see Fig. 7(b)]. Note that the central area has a surficial mud layer of 11–12 m, whereas the NW part of the main acoustic track has a variable mud layer thickness of 7–10 m.

Along the E-W transect, the surficial mud layer thickness reduces from 6–8 m (PC54 and 55) to 2–3 m (PC52). Results from PC54 and

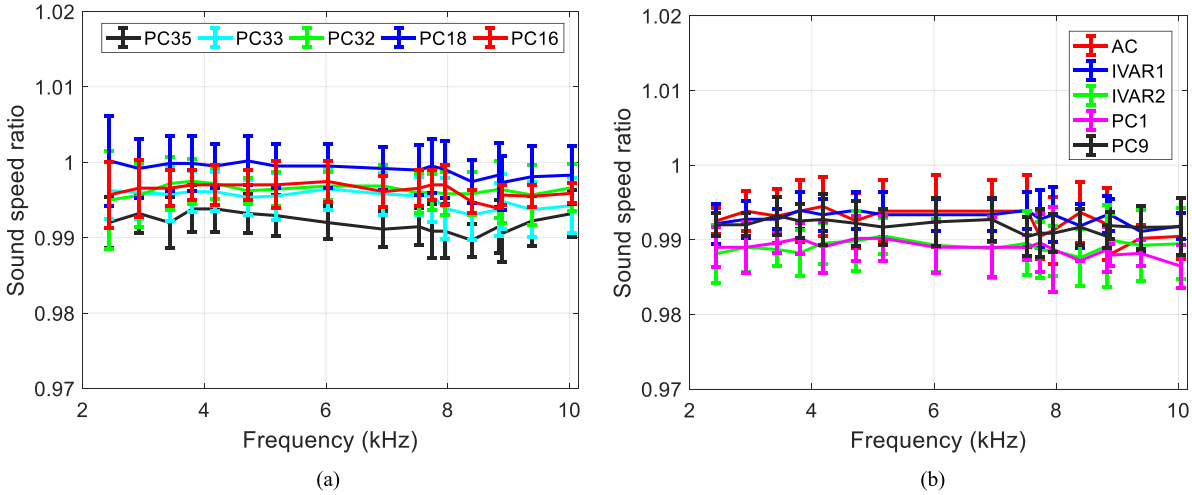

Fig. 7. Sediment sound-speed ratio in the frequency band of 2–10 kHz at (a) five sites in the central area and (b) five sites along the NW part of the main propagation track. Penetration depths are listed in Table I.

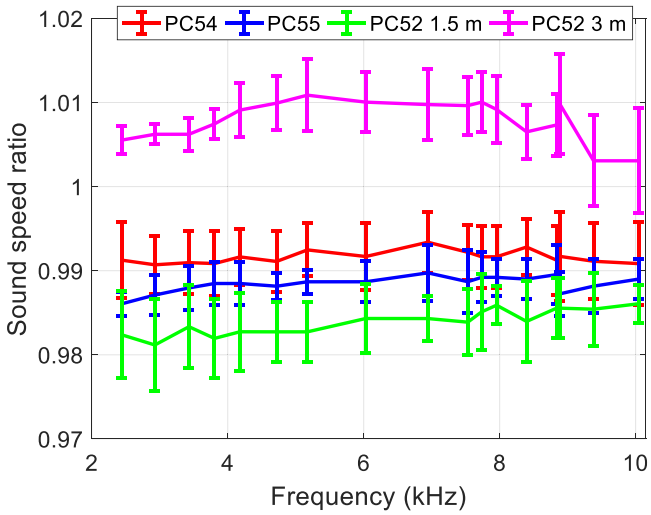

Fig. 8. Sediment sound-speed ratio in the frequency band of 2–10 kHz along the middle E-W transect. Note, at PC52, data were taken at two penetration depths: 1.5 and 3 m. With surficial mud layer thinning and the emerging sandy intrusion, sound-speed ratio at 3 m is about 3% more than that at 1.5 m.

PC55 (see Fig. 8) are similar to those from the NW part of the main track [see Fig. 7(b)]. At PC52, the chirp sonar data indicate that the intruding sandy basement is about 2–3 m below the water–sediment interface. To investigate sound-speed depth dependence, data were taken at 1.5 and 3 m penetration depths. The first 1.5 m has a sound-speed ratio of 0.983, whereas at 3 m, the averaged sound-speed ratio increases to about 1.01 due to greater sand content (see Fig. 8).

The most pronounced sound-speed variation is in the "sand box" area in the southwest corner of the study area. The surficial mud layer thickness varies from about 1–2 m near VC1 location to about 6 m at VC8. A track was chosen to follow VC1, 2, 4, 6, and 8. At all five sites, two penetration depths, approximately 1.5 and 3 m, were employed to investigate the variation of sediment properties over depth.

At 1.5-m penetration depth, the sound-speed ratio is about unity for the first two sites with the thinnest surficial mud layers VC1 and VC2 [see Fig. 9(a)]. As the surficial mud layer thickness increases from VC4 to VC8, Fig. 9(a) shows a trend of decreasing sound speed. VC6 and VC8 have the lowest sound-speed ratio among the five sites, about 0.98. As SAMS penetrates to 3 m, the variation in sound speed increases significantly. At VC1, penetration into the sandy layer is the greatest and, therefore, it has the highest sound-speed ratio of 1.07. From VC1 to VC8, sound speed measured at 3 m steadily decreases due to the decreasing sand content. VC8 has a thick enough mud layer that there is no direct penetration into the intruding sandy basement. The sound-speed ratio at VC8 is 0.99 at 3-m penetration, just slightly higher than 0.98 measured at 1.5 m.

One interesting trend in sound-speed ratio over the four priority areas was observed from west to east. The measured sound-speed ratio on the west side of the study area (PC52, VC6, and VC8 at 1.5-m penetration depth) is observed to be the lowest at the study site, with mean values about 0.98. In between E-W transect and NW part of the main track (from PC54 to IVAR1), the mean sound-speed ratio increases to about 0.99. Further east, the sound-speed ratio in the central area continues to increase to about 0.995. This is consistent with observations by Twichell and McClennen [39] of the steady fining of surface sediment to the west based on the data of Hathaway.

C. Simple Two-Layer Model for Sites With Incremental Penetration Depths

One central question of SBCEX17 is: What is the impact of sediment inhomogeneity on sound propagation in mud? An important aspect of sediment inhomogeneity is sound-speed variation over depth. SAMS data allow a simple way to investigate such depth dependence by comparing results measured at different depths. There are two types of depth dependence at SBCEX17 sites: one is the sound-speed gradient potentially due to overburden pressure or compaction in mud and the other is the sound-speed gradient due to intruding sandy materials.

The former corresponds to sites with a thick mud layer, such as PC33, IVAR2, PC54, and VC8, where sediment geoacoustic properties were measured at two depths to investigate vertical structures. Fig. 10 shows the results of path-averaged sediment sound-speed ratio at the four sites, with the red curve representing the shallow penetration and the blue for the deep. The mean sound-speed ratio results show a trend of increasing sound-speed ratio at deeper penetration depths, with overlapping uncertainty bounds at some frequencies. Note that these

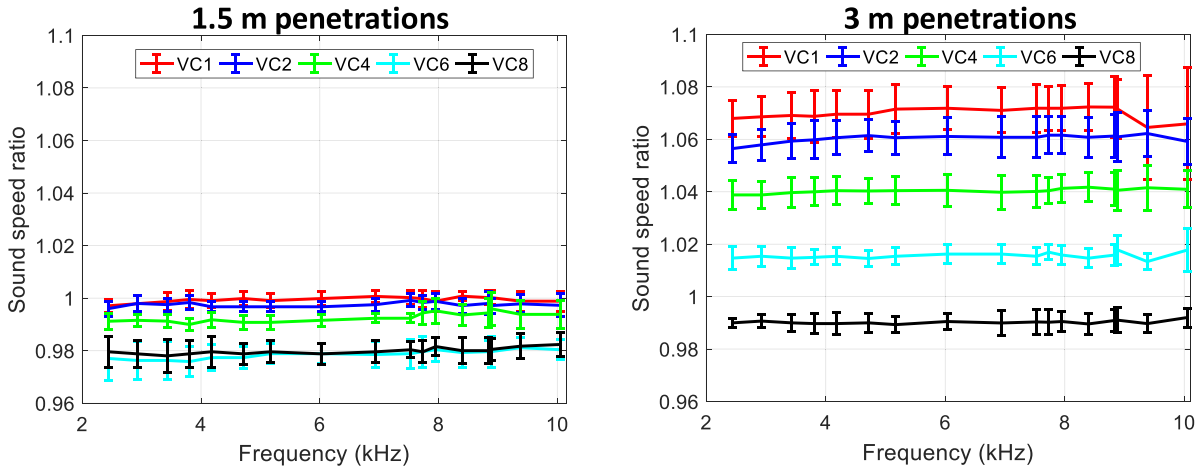

Fig. 9. Sound-speed ratio in the "sand box" area, the SW corner of the SBCEX17 site. Five sites were chosen: VC1, 2, 4, 6, and 8 to map out the shallowest sandy intrusion at VC1 to the total disappearance of it at VC8. At all five sites, data were taken at penetration depths of 1.5 m (left) and 3 m (right).

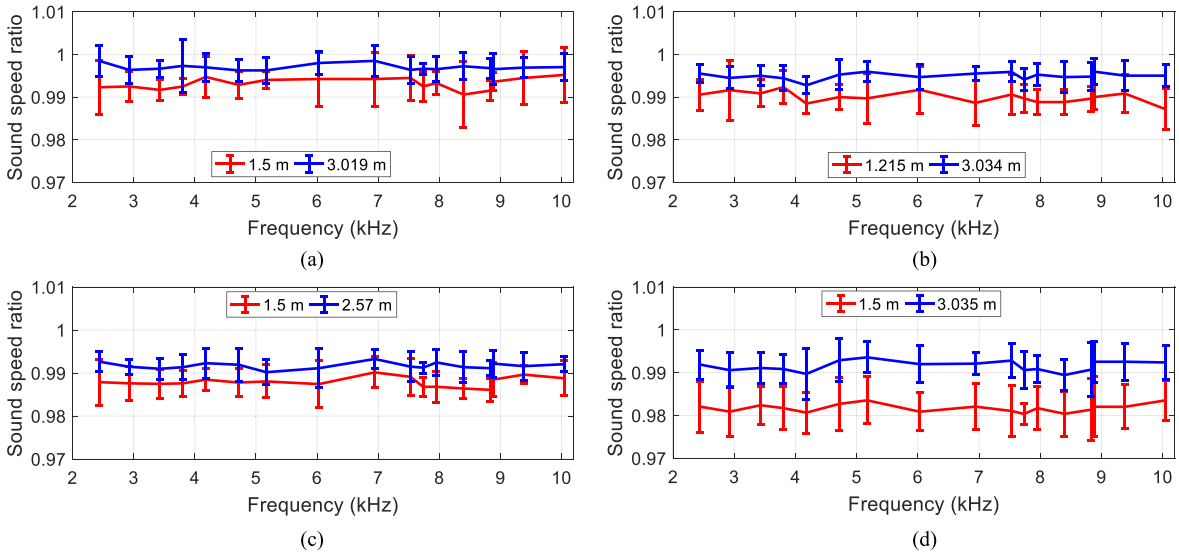

Fig. 10. Sediment sound-speed ratio at (a) PC33, (b) PC54, (c) IVAR2, and (d) VC8.

four sites have mud layer thickness greater than 5 m based on the chirp data. For VC8, although the chirp data indicate that the surficial mud layer can be 5 m thick, an increase in sandy content may contribute to the two well-separated sound-speed ratio curves at penetration depths of 1.5 and 3.035 m.

Conceptually, path-averaged sediment sound speed can be estimated straightforwardly by measuring the distance and travel time between a source and a receiver, as has been done so far (see Figs. 7–10). Using the sound-speed results integrated over the propagation path, however, the sound speed for the deeper sediment can be underestimated, as will be shown next.

A simple diagram, in Fig. 11, is shown to demonstrate the measurement geometry and the meaning of sound speed shown so far. In Fig. 11, c_1 represents the path-averaged sound speed from the source to the receiver at the first penetration depth h_1 (path length r), whereas c represents that from the source to the receiver at the second penetration depth $h_1 + h_2$ (path length R). Here, h_1 and h_2 are usually about 1.5 m, i.e., data were taken at 1.5 and 3 m. The path lengths of the nine source–receiver pairs range from 1.9–3.4 m for r and 3.2–4.2 m for R. The sound-speed results shown in Figs. 7–10 are path-averaged sound-speed results c_1 for layer 1 and c, the path-averaged sound speed over both layers. If the sound speed c_2 in the lower layer is higher than c_1, the overall sound speed c will be higher than c_1, but lower than c_2. Note that the word "layer" here only refers to the two parts of the sediment bounded by SAMS penetration depths and has nothing to do with physical bottom layers.

Using this simple two-layer fluid model (see Fig. 11), one may obtain the mean sound speed c_2 for the lower layer, with c_1 as an input. Ray bending will be neglected in the two-layer model, as worst case calculations show negligible ray bending effects. Ray bending must be considered only when the two "layers" are distinctly different, and the worst case is for the greatest source–receiver separation. Taking the greatest horizontal and vertical separations to be 3 m, the change in time delay due to ray bending is less than 0.2% using exaggerated sound speeds of 1450 and 1650 m/s for layers 1 and 2. This simple model is meant to give a crude estimation of sediment sound-speed

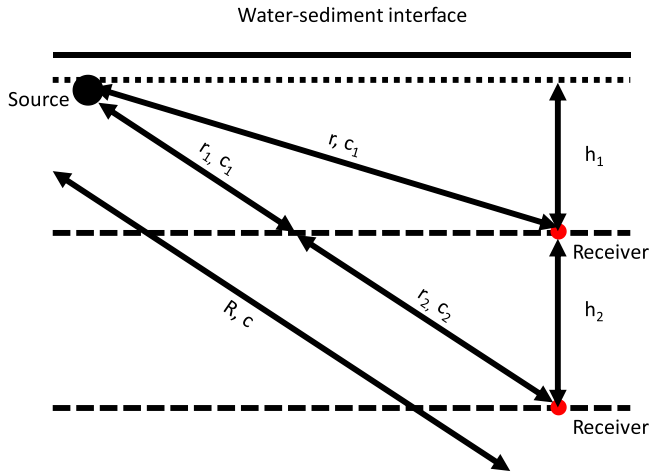

Fig. 11. Diagram of a simple fluid two-layer model for sites with data taken at two depths, providing averaged sound speed within each layer. Note: this two-layer model does not correspond to a physical bottom model. Here, r_1, r_2, r, and R are path lengths, and the accompanying c_1, c_2, and c show mean sound speed along the paths.

variation as a function of depth. More sophisticated modeling will be carried out in the future to extract vertical profiles using the ten pairs of source–receiver geometries.

Following Fig. 11, sound speed c_1 can be obtained using data taken at penetration depth h_1 with propagation distance r; similar for the overall mean sound speed c at penetration depth $h_1 + h_2$, with propagation distance R. Then, c_2 can be obtained using the relation

$$c = \frac{r_1 + r_2}{t} = \frac{r_1 + r_2}{\frac{r_1}{c_1} + \frac{r_2}{c_2}}$$

where t is the signal arrival time, and r_1 and r_2 are propagation paths in layers 1 and 2 with $R = r_1 + r_2$. Therefore

$$c_2 = \frac{r_2}{\frac{r_1 + r_2}{c} - \frac{r_1}{c_1}}$$

With $r_1/r_2 = h_1/h_2$, we can find

$$c_2 = \frac{1}{\frac{\frac{h_1}{h_2} + 1}{c} - \frac{\frac{h_1}{h_2}}{c_1}}.$$

After applying the two-layer model, the sound speeds c_1 and c_2 can be obtained. Fig. 12 uses the same data as in Fig. 10, but instead of giving a path-averaged sound speed c for the deeper penetration, it provides a sound speed c_2 in the lower layer. The first layer results are identical to those in Fig. 10. Though a very crude way to look at the vertical structure of sediment sound speed, the sound speed for the lower layer should be closer to its true value. All sites that have data at more than one penetration depths were recalculated using the two-layer model. The sound speeds in the so-called "sand box" area produce even greater difference among sites from VC1 to VC8 (see Fig. 13), if compared with the right panel of Fig. 9.

IV. Proposed Bottom Sound-Speed Model: Linear Versus Exponential

In fine-grained sediments, the vertical structure of sediment geoacoustic properties is crucial for geoacoustic modeling purposes [9]. Using the SAMS sediment sound-speed results taken at different depths, a preliminary study of the sound-speed structure at the SBCEX17 site is presented in this section.

Here, data are restricted for those taken at the deep mud sites, i.e., with surficial mud layer thickness greater than 5–6 m. There are a total of 14 such sites, and among them, four sites have data at two penetration depths. Combined sediment sound-speed ratios from the 14 sites are shown as a function of measurement depths in Fig. 14. The measurement depth (not penetration depth as will be explained next) ranges from 1–3.1 m, with the sinking depth 0.4 m taken into account.

As noted earlier, for all deployments in SBCEX17, SAMS sank into the sediment by 30–50 cm. For sites that only have one penetration depth, sediment sound-speed ratio represents the averaged sound speed from about 40 cm beneath the water sediment interface (where the source was) down to the receiver. For sites that have two penetration depths, the two-layer model was used to find the averaged sound speed within each layer. Measurement depth represents the middle depth of each layer where the measurement was conducted, with the sinking depth included (0.4 m). The measurement depth can be calculated using the source/receiver depths in Table I: for deployments with one penetration depth, it is simply the average of source and receiver depths, whereas for sites with multiple penetration depths, the measurement depth for the second or third layer is the average of first and second receiver depths or that of second and third receiver depths. Again, the layers here are bounded by penetration depths and they are not related to physical bottom layers.

Two simple bottom sound-speed models, one exponential and the other linear, were obtained as best fits to all the SAMS path-averaged sound-speed results (see Fig. 14). Their expressions are

$$c_{\text{exp}} = 1382.8 + 83.9 \times \left(1 - e^{-1.611 \times z}\right)$$

and

$$c_{\text{lin}} = 1446.3 + 7.7 \times z.$$

All parameters here represent best fit parameters between model and data using the criteria of minimum RMSE. RMSE for the linear and exponential fits are 0.00521 and 0.00502, respectively, with the exponential model lower by 3.7%. The statistical significance between the two models was tested using Welch's t-test, with the data/model errors for both models as paired samples. The two models are indeed statistically distinguishable at 96.8% confidence level.

The linear model here shows a $7.7s^{-1}$ sound-speed gradient, in comparison to a site-averaged linear sound-speed gradient of $9s^{-1}$ within the surficial 10-m mud layer [40]. Within the SAMS measurement depth range of 1–3.1 m, sound-speed ratio shows a trend of increase to approximately 1.5 m and majority of data remain in the range of 0.995–1 between 1.6 and 3.1 m. Subject to the assumptions used in this analysis, it appears that the SAMS data favor the nonlinear model. Larger gradients are observed at depth less than 1.5 m, and the nonlinear model describes this behavior. These results should be compared with other measurement techniques to constrain sediment geoacoustic properties near the water–sediment interface and for depth greater than 3 m. In addition, the differences in mud properties among measurement sites need to be considered in the development of the bottom model.

V. Summary

During SBCEX17, SAMS was successfully deployed at a total of 18 sites. These sites were chosen to measure sediment geoacoustic properties in mud and also in the intruding sandy basement for acoustic modeling purposes. The four priority areas are as follows:

1) the central area;

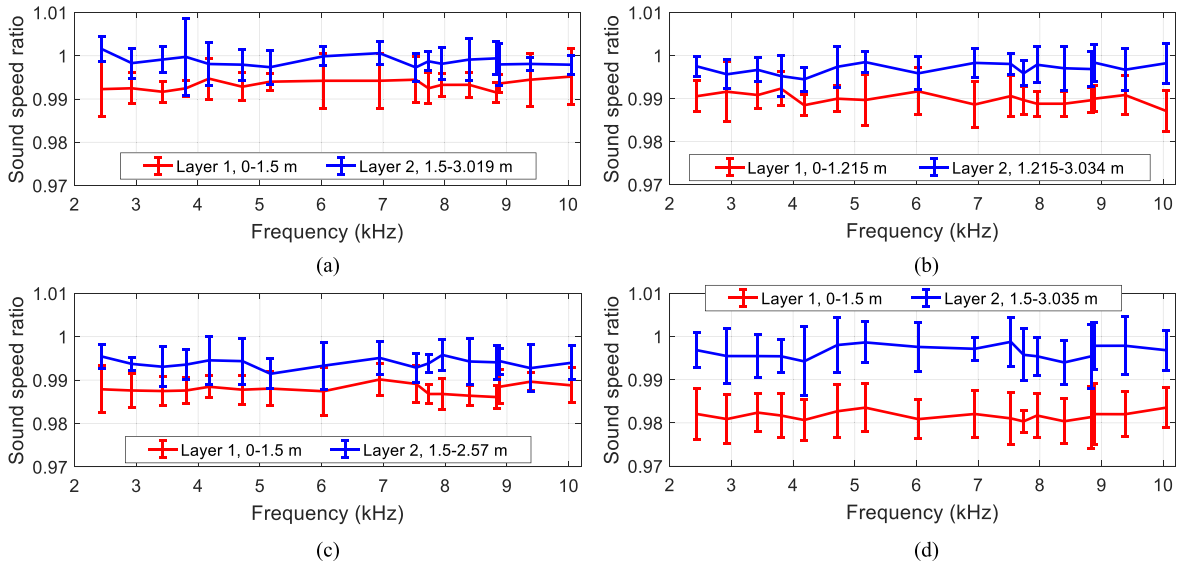

Fig. 12. Sediment sound-speed ratios in layers 1 and 2, using the two-layer model. (a) PC33. (b) PC54. (c) IVAR2. (d) VC8. Same data as shown in Fig. 10.

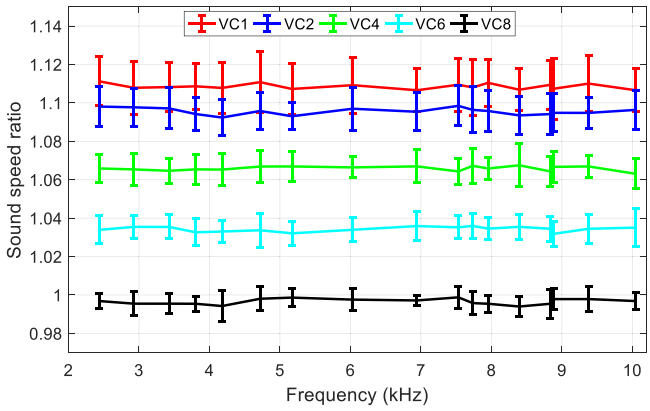

Fig. 13. Averaged sound-speed ratios for the second layer for VC1, VC2, VC4, VC6, and VC8 after applying the two-layer model (in comparison with Fig. 9, right panel, the overall mean sound speed).

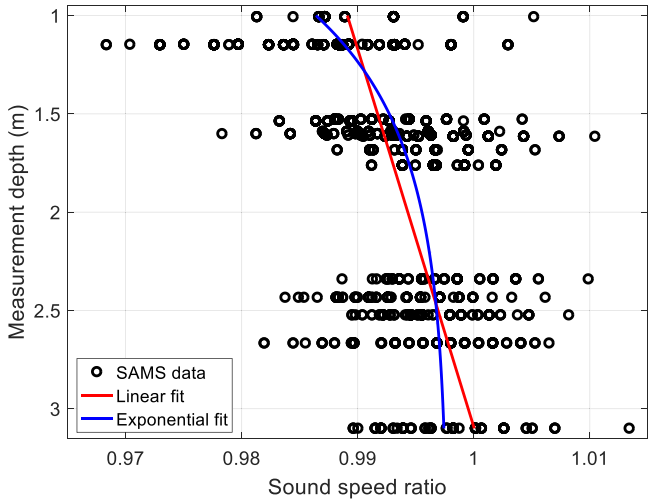

Fig. 14. Depth dependence of sediment sound-speed ratio in surficial mud layer. Results use all sound speeds obtained using the 2–3-kHz Gaussian signal. Both linear and exponential curves are best fits to SAMS results using the criteria of minimum root-mean-square error (RMSE). The exponential model has an RMSE of 0.00502 that is 3.7% lower than the linear.

2) NW part of the main acoustic track;
3) E-W transect with transition into shallow mud layer;
4) the "sand box" area with sandy intrusion about 1.5 m below the water–sediment interface.

In this article, path-averaged sediment sound speed in the frequency range of 2–10 kHz is presented for the four priority areas using the time-of-flight method. In general, there is little dispersion in mud between 2 and 10 kHz. Along the main acoustic track, slight spatial variation in sound speed can be observed. Measurements at the five sites in the central area yield similar sound-speed ratios with the mean in the range of 0.99–1. For sites along the NW part of the main acoustic track, the overall sound-speed ratio is less than that in the central area by 0.005 or 0.5%.

For sites with apparent sandy intrusions, including the E-W transect and the "sand box" areas, results for the surficial mud layer are similar to those from the NW part of the main track. For sandy intrusion sites, such as at PC52 and VC1-VC6, data were taken at penetration depths of 1.5 and 3 m to investigate the sound-speed variation as a function of depth. A two-layer model was applied to data taken from these sites and the mean sound speeds c_1 and c_2 within each layer were obtained.

Among the sites with clear sand intrusion, the most pronounced sound-speed variation is in the "sand box" area. The surficial mud layer varies in thickness from about 1–2 m near VC1 to about 6 m at VC8. At the penetration depth of 1.5 m, VC1 and VC2, with the shallowest mud layer, have sound-speed ratios about unity. As the surficial mud layer thickness increases from VC4 to VC8, a trend of decreasing sound-speed ratio is observed. VC6 and VC8 have the lowest sound-speed ratio among the five sites, about 0.98. At 3 m, the variation in sound-speed ratio increases significantly. At VC1, with penetration into the underlying sandy intrusion, the sound-speed ratio is the highest, about 1.105. From VC1 to VC8, sound-speed ratio steadily decreases due to less sandy content in the surficial 3 m. VC8 has a thick enough mud layer

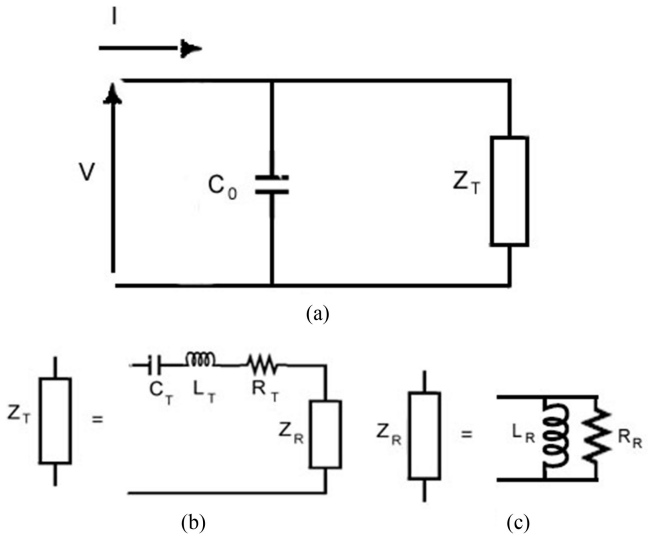

Fig. 15. (a) Transducer equivalent circuit with a parallel combination of capacitor Co and impedance Z_T, which is comprised of a sum of (b) mechanical and radiation impedances. (c) Radiation impedance represented by a parallel inductor–resistor combination.

that there is no direct penetration into the intruding sandy basement so it only shows a slightly increased sound-speed ratio of 0.995, compared to 0.98 at 1.5-m penetration.

Using the path-averaged sound-speed results taken at different depths in mud, a preliminary bottom sound-speed model is proposed. It appears that the SAMS data favor the nonlinear bottom sound-speed model over the linear and larger gradients are observed at depths shallower than 1.5 m. This observation should be compared with other measurements, such as cores, chirp sonar, and the angle of intromission, to constrain sediment geoacoustic properties near the water–sediment interface and for depths greater than 3 m, to facilitate the development of a geoacoustic model at the study site.

APPENDIX
TRANSDUCER MODELING INCLUDING BURIAL EFFECTS

As the sources were buried 30–50 cm into surficial sediments, there is a concern that a time shift relative to operation in water could bias sound-speed determinations. To address this problem, a model was developed and used to predict source behavior in water and sediment. Additionally, a similar model was used to look for time shifts in reception. The transducer modeling effort presented here is similar to that developed by Buckingham and Richardson [13], who examine the pulse-distorting effects of mechanical resonance and loading by the surrounding medium. The present effort emphasizes the differences between in-water and in-sediment transducer behavior.

The transducer model employs the equivalent circuit (see Fig. 15) in which the capacitance of the transducer is denoted as C_0. The other circuit elements are nonelectrical and the transformer used to convert their mechanical and radiation properties into electrical properties are omitted [41], that is, the model gives their equivalent electrical properties as manifested at the transducer terminals. These include spring constant (C_T), mass (L_T), and dissipation (R_T). The radiation properties are represented by the parallel combination of L_R and R_R. This departs from the use of a series combination [13], [41] and has the advantage that the values of L_R and R_R are independent of frequency for spherical transducers. No attempt was made to fix the model parameters based on dimensions and physical properties. Rather, they were determined by fitting the model to admittance measurements (*I*/*V*, with reference to Fig. 15) made over frequencies up to 50 kHz. The values of the model circuit elements for the ITC 1032 and ITC 1007 transducers are given in Table II.

TABLE II
EQUIVALENT CIRCUIT PARAMETERS

Transducer	C_0 (F)	C_T (F)	L_T (H)	R_T (Ω)	L_R (H)	R_R (Ω)
1032	1.89×10^{-8}	9.08×10^{-9}	0.00235	3.92	0.532	187
1007	6.02×10^{-8}	2.85×10^{-8}	0.00653	2.66	1.18	150

Using the equivalent circuit of Fig. 15, the ratio of complex pressure P at range r to voltage V is

$$\frac{P}{V} = \frac{1}{r}\sqrt{\frac{\rho c}{4\pi R_R}}\frac{Z_R}{Z_T}. \tag{1}$$

Using recorded replicas of the transmitter voltage, this complex transfer function will give the time dependence of the in-water pressure at range r. If the source is buried in sediment, the change in the transfer function can be found by scaling various parameters by the sediment density and sound-speed ratios, i.e., a_ρ and ν. Specifically, ρ and c inside the radical above are replaced by $a_\rho\,\rho$ and νc, whereas R_R is replaced by $a_\rho \nu R_R$, and L_R is replaced by $a_\rho\, L_R$. For the simulations to be presented, the following acoustic parameters were used: $c = 1470$ m/s, $a_\rho = 1.6$, and $\nu = 0.99$.

The model results presented in Figs. 16 and 17 use the same transmitted signal as in the sea trial, and in this case, the 2–3-kHz Gaussian pulse was used for both ITC1032 and ITC1007. For both sources, modeling results are consistent with field data (see Fig. 5) that an increase in amplitude after insertion in the sediment is observed [see Figs. 16(a) and 17(a)]. The reason for this increase cannot be seen by simple inspection of (1), but consideration of the underlying physical model shows that the factor inside the radical is independent of the acoustic impedance ρc, whereas Z_R is nearly proportional to ρc. The greater density of sediment compared to water thus accounts for the increase in amplitude. For this article, the most important output of the model is the phase delay for sources immersed in sediment with respect to that in water. ITC1032 shows little phase delay, i.e., $\sim$1 μs [see Fig. 16(b)], whereas ITC1007 shows a phase delay range of 2.5–4 μs. For propagation paths of 2–4.3-m range, this phase delay would cause a maximum of 0.3% correction to the sound speed (an increase in measured sound speed after the delay is removed). Phase delay results were included in the sound-speed calculations in this article.

The same concern regarding time delays upon insertion into the sediment applies to the SAMS receiver (ITC5510). The equivalent circuit model can be used to predict the complex receiving response, provided it is supplemented with a factor known as the diffraction constant [42]. Two issues stand in the way of applying the model: first, owing to the interaction of the ring transducer with the drill shaft, the receiver geometry is not one of the simple types for which the diffraction constant is known. Second, no admittance measurements have been made on this transducer, so the model parameters are not known. As an interim approach, the ITC1007 parameters and the diffraction constant for spherical transducers have been used with the result that amplitude and time shifts are found to be negligible for sediment insertion. In support of this conclusion, the assumption of spherical symmetry in the model was removed, giving the model an extra variable parameter. After fitting this model to the measured receiving sensitivity as a function of frequency, amplitude and time shifts again were found to be negligible.

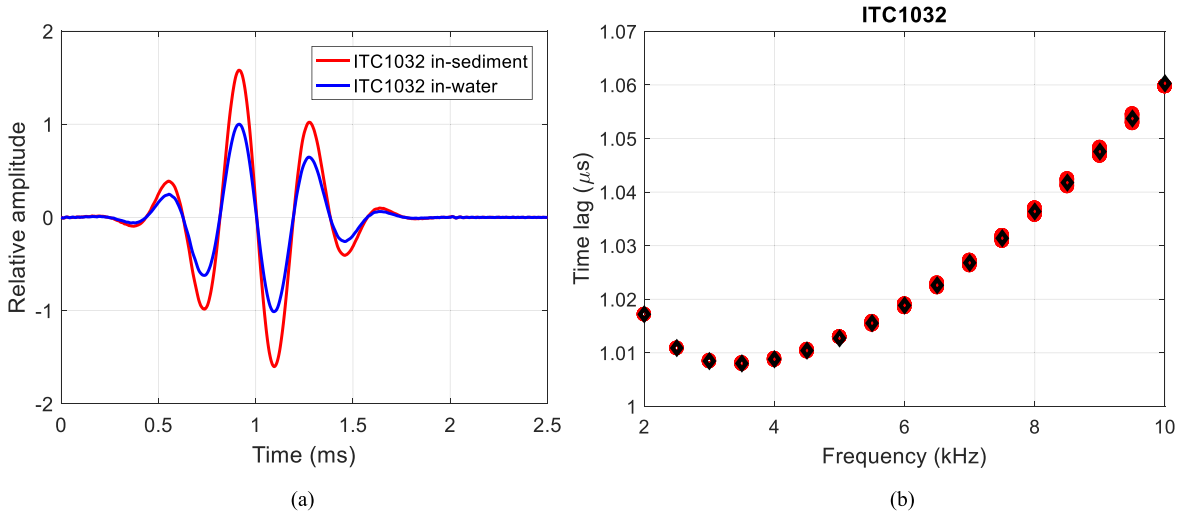

Fig. 16. (a) Model waveforms and (b) modeled time lag for transmitted pressure with a source in water and sediment with center frequency 2.5 kHz for the ITC 1032 transducer.

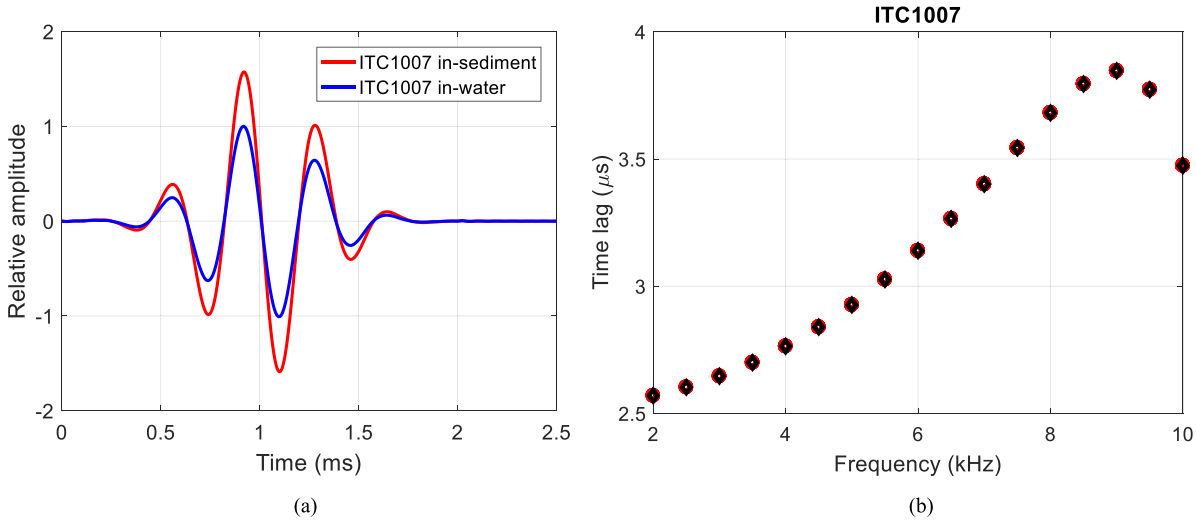

Fig. 17. Model waveforms and (b) modeled time lag for transmitted pressure with a source in water and sediment with center frequency 2.5 kHz for the ITC 1007 transducer.

ACKNOWLEDGMENT

The authors would like to thank the engineering team of N. Michel-Hart, B. Brand, and P. Aguilar for their expertise and dedication during the field trial. They would also like to thank the *R/V Sharp* crew for providing all the support during the experiment.

REFERENCES

[1] E. L. Hamilton, G. Shumway, H. W. Menard, and C. J. Shipek, "Acoustic and other physical properties of shallow-water sediments off San Diego," *J. Acoust. Soc. Amer.*, vol. 28, pp. 1–15, 1956.

[2] E. L. Hamilton, "Sediment sound velocity measurement made in-situ from bathyscaph Trieste," *J. Geophys. Res.*, vol. 68, pp. 5991–5998, 1963.

[3] L. D. Hampton, "Acoustic properties of sediments," *J. Acoust. Soc. Amer.*, vol. 42, pp. 882–890, 1967.

[4] E. L. Hamilton, H. P. Bucker, D. L. Keir, and J. A. Whitney, "Velocities of compressional and shear waves in marine sediments determined in situ from a research submersible," *J. Geophys. Res.*, vol. 75, pp. 4039–4049, 1970.

[5] E. L. Hamilton, "Sound velocity gradients in marine sediments," *J. Acoust. Soc. Amer.*, vol. 65, pp. 909–922, 1979.

[6] A. L. Anderson and L. D. Hampton, "Acoustics of gas-bearing sediments I. Background," *J. Acoust. Soc. Amer.*, vol. 67, pp. 1865–1889, 1980.

[7] A. L. Anderson and L. D. Hampton, "Acoustics of gas-bearing sediments II. Measurements and models," *J. Acoust. Soc. Amer.*, vol. 67, pp. 1890–1903, 1980.

[8] E. L. Hamilton, "Sound velocity as a function of depth in marine sediments," *J. Acoust. Soc. Amer.*, vol. 78, pp. 1348–1355, 1985.

[9] E. L. Hamilton, "Geoacoustic modeling of the sea floor," *J. Acoust. Soc. Amer.*, vol. 68, pp. 1313–1340, 1980.

[10] E. I. Thorsos *et al.*, "An overview of SAX99: Acoustic measurements," *IEEE J. Ocean. Eng.*, vol. 26, no. 1, pp. 4–25, Jan. 2001.

[11] M. D. Richardson *et al.*, "Overview of SAX99: Environmental considerations," *IEEE J. Ocean. Eng.*, vol. 26, no. 1, pp. 26–53, Jan. 2001.

[12] R. D. Stoll, "Velocity dispersion in water-saturated granular sediment," *J. Acoust. Soc. Amer.*, vol. 111, no. 2, pp. 785–793, 2002.

[13] M. J. Buckingham and M. D. Richardson, "On tone-burst measurements of sound speed and attenuation in sandy marine sediments," *IEEE J. Ocean. Eng.*, vol. 27, no. 3, pp. 429–453, Jul. 2002.

[14] K. B. Briggs, D. Tang, and K. L. Williams, "Characterization of interface roughness of rippled sand off Fort Walton Beach, Florida," *IEEE J. Ocean. Eng.*, vol. 27, no. 3, pp. 505–514, Jul. 2002.
[15] D. Tang, K. B. Briggs, K. L.Williams, D. R. Jackson, E. I. Thorsos, and D. B. Percival, "Fine-scale volume heterogeneity measurements in sand," *IEEE J. Ocean. Eng.*, vol. 27, no. 3, pp. 546–560, Jul. 2002.
[16] A. H. Reed, K. B. Briggs, and D. L. Lavoie, "Porometric properties of sand from SAX99 derived from traditional measurements and image analysis/network modeling," *IEEE J. Ocean. Eng.*, vol. 27, no. 3, pp. 581–592, Jul. 2002.
[17] M. D. Richardson, K. L.Williams, K. B. Briggs, and E. I. Thorsos, "Dynamic measurement of sediment grain compressibility at atmospheric pressure: Acoustic applications," *IEEE J. Ocean. Eng.*, vol. 27, no. 3, pp. 593–601, Jul. 2002.
[18] P. C. Hines, J. C. Osler, J. G. E. Scrutton, and L. J. S. Halloran, "Time-of flight measurements of acoustic wave speed in a sandy sediment at 0.6–20 kHz," *IEEE J. Ocean. Eng.*, vol. 35, no. 3, pp. 502–515, Jul. 2010.
[19] J. Yang, D. Tang, and K. L. Williams, "Direct measurement of sediment sound speed in Shallow Water '06," *J. Acoust. Soc. Amer.*, vol. 124, pp. EL116–EL121, 2008.
[20] A. Turgut and T. Yamamoto, "In situ measurements of velocity and attenuation in New Jersery Shelf sediments," *J. Acoust. Soc. Amer.*, vol. 124, pp. EL122–EL127, 2008.
[21] J. Yang and D. Tang, "Direct measurements of sediment sound speed and attenuation in the frequency band of 2–8 kHz at the Target and Reverberation Experiment site," *IEEE J. Ocean. Eng.*, vol. 42, no. 4, pp. 1102–1109, Oct. 2017, doi: 10.1109/JOE.2017.2714722.
[22] B. T. Hefner, "Inversion of high frequency acoustic data for sediment properties needed for the detection and classification of UXOs," Dept. Def., Strategic Environ. Res. Develop. Program, Alexandria, VA, USA, SERDP Project MR-2229, 2015. [Online]. Available: https://www.serdp-estcp.org/Program-Areas/Munitions-Response/Munitions-Underwater/MR-2229/MR-2229
[23] A. Barbegelata *et al.*, "ISSAMS: An in situ sediment acoustic measurement system," in *Shear Waves in Marine Sediments*. J. M. Hoven, M. D. Richardson, and R. D. Stoll, Eds. Dordrecht, The Netherlands: Kluwer, 1991.
[24] A. I. Best, Q. J. Huggett, and A. J. K. Harris, "Comparison of in situ and laboratory acoustic measurements on Lough Hyne marine sediments," *J. Acoust. Soc. Amer.*, vol. 110, pp. 695–709, 2001.
[25] G. B. N. Robb *et al.*, "Measurement of the in situ compressional wave properties of marine sediments," *IEEE J. Ocean. Eng.*, vol. 32, no. 2, pp. 484–496, Apr. 2007.
[26] M. A. Biot, "Theory of propagation of elastic waves in a fluid-saturated porous solid. I. Low-frequency range," *J. Acoust. Soc. Amer.*, vol. 28, pp. 168–178, 1956.
[27] M. A. Biot, "Theory of propagation of elastic waves in a fluid-saturated porous solid. II. Higher frequency range," *J. Acoust. Soc. Amer.*, vol. 28, pp. 179–191, 1956.
[28] K. L. Williams, "An effective density fluid model for acoustic propagation in sediments derived from Biot theory," *J. Acoust. Soc. Amer.*, vol. 110, pp. 2276–2281, 2001.
[29] M. J. Buckingham, "Compressional and shear wave properties of marine sediments: Comparisons between theory and data," *J. Acoust. Soc. Amer.*, vol. 117, pp. 137–152, 2005.
[30] N. P. Chotiros and M. J. Isakson, "A broadband model of sandy ocean sediments: Biot-Stoll with contact squirt flow and shear drag," *J. Acoust. Soc. Amer.*, vol. 116, pp. 2011–2022, 2004.
[31] T. J. Gorgas *et al.*, "In situ acoustic and laboratory ultrasonic sound speed and attenuation measured in hererogeneous soft seabed sediments: Eel River shelf, California," *Mar. Geol.*, vol. 182, pp. 103–119. 2002.
[32] K. M. Lee *et al.*, "Preliminary characterization of surficial sediment acoustic properties and infauna in the New England Mud Patch," *J. Acoust. Soc. Amer.*, vol. 139, pp. 2111–2111, 2016.
[33] A. D. Pierce, W. L. Siegmann, and E. Brown, "Analytical discussion of past measurements of acoustic attenuation in mud sediments and of possible future experimental approaches," *Proc. Meetings Acoust.*, vol. 25, 2015, Art. no. 005001. [Online]. Available: https://doi.org/10.1121/2.0000221
[34] E. M. Brown, A. D. Pierce, and W. L. Siegmann, "Viscosity-based theory of phase velocity and attenuation of sound in mud consisting of water and flocculated clay particles," *J. Acoust. Soc. Amer.*, vol. 144, 2018, Art. no. 1981. [Online]. Available: https://doi.org/10.1121/1.5068648
[35] J. A. Goff, A. H. Reed, G. Gawarkiewicz, P. S. Wilson, and D. P. Knobles, "Stratigraphic analysis of a sediment pond within the New England Mud Patch: New constraints from high-resolution chirp acoustic reflection data," *Mar. Geol.*, vol. 412, pp. 81–94, Jun. 2019.
[36] J. A. Goff, J. D. C. A. H. Reed, S. Liu, P. S. Wilson, and D. P. Knobles, "The coarse- to fine-grained boundary beneath the New England Mud Patch: Evidence from seismic and core data for an abrupt post-transgressive change in hydrologic regime on the continental shelf," in *Proc. Amer. Geophys. Union Fall Meeting*, Dec. 2016, abstract #EP24B-01.
[37] J. D. Chaytor, "Measurements of geologic characteristics, geophysical properties, and geoacoustic response of sediments from the New England Mud Patch," presented at the 2nd Post-Exp. Workshop Seabed Characterization Exp., Appl. Phys. Lab., Seattle WA USA, 30–31 May, 2017.
[38] M. S. Ballard *et al.*, "In situ measurements of compressional wave speed and attenuation during gravity coring operations in the New England Mud Patch," *IEEE J. Ocean. Eng.*, 2019, doi: 10.1109/JOE.2019.2924560.
[39] D. C. Twichell and C. E. McClennen, "Morphology and processes associated with the accumulation of the fine-grained sediment deposit on the southern New England shelf," *J. Sedimentary Petrology*, vol. 51, pp. 269–280, 1981.
[40] D. P. Knobles *et al.*, "Maximum entropy derived statistics of sound-speed structure in a fine-grained sediment inferred from sparse broadband acoustic measurements on the New England continental shelf," *IEEE J. Ocean. Eng.*, 2019, doi: 10.1109/JOE.2019.2922717.
[41] C. H. Sherman and J. L. Butler, *Transducers and Arrays for Underwater Sound*. New York, NY, USA: Springer, 2007.
[42] T. A. Henriquez, "Diffraction constants of acoustic transducers," *J. Acoust. Soc. Amer.*, vol. 36, pp. 267–269, 1964.

Jie Yang received the B.S. degree in physics from the Ocean University of Qingdao, Qingdao, China, in 1999, and the Ph.D. degree in mechanical engineering from Georgia Institute of Technology, Atlanta, GA, USA, in 2007.

Since 2007, she has been a Postdoctoral Fellow supported by the U.S. Office of Naval Research. She is currently a Principal Physicist with the Applied Physics Laboratory, University of Washington, Seattle, WA, USA. Her research interests include both active and passive acoustics, with the former focusing on midfrequency sound propagation and reverberation in littoral oceans and the latter on estimating wind speed and rain rate using ocean ambient sound and their relation to global water cycle and climate change.

Darrell R. Jackson received the B.S., M.S., and Ph.D. degrees in electrical engineering from the University of Washington, Seattle, WA, USA, in 1960, 1963, and 1966, respectively, and the Ph.D. degree in physics from California Institute of Technology, Pasadena, CA, USA, in 1977, with a dissertation on the extraction of experimental predictions from quark–gluon theory.

His thesis research was directed toward applications of magnetic resonance. He was a Research Engineer with Boeing and later on joined the faculty of the University of Massachusetts, Amherst, MA, USA. Since joining the Applied Physics Laboratory (APL), University of Washington, in 1976, his research has centered on underwater acoustics. Since retirement in 2000, he has continued his research as a Senior Fellow at APL and coauthored the book *High-Frequency Seafloor Acoustics* with M. D. Richardson (Springer-Verlag, 2007). His research interests include sound scattering by the seafloor, including inversions of scattering data for sensing of seafloor properties.

Dr. Jackson is a Fellow and Silver Medalist of the Acoustical Society of America.